DINCON'09
8TH BRAZILIAN CONFERENCE ON DYNAMICS, CONTROL AND APPLICATIONS
MAY 18-22, 2009

HOW MUCH IS THE SPATIO-TEMPORAL DATA ASYMMETRY AFFECTED BY A COMPACT WAVELET RECONSTRUCTION?

Thalita Biazzuz Veronese[1], *Margarete Oliveira Domingues*[2], *Odim Mendes*[3], *Reinaldo Roberto Rosa*[4]

[1]Pós Graduação em Computação Aplica (CAP/INPE), São José dos Campos - São Paulo, Brazil, thalita@lac.inpe.br
[2,4]Laboratório de Computação e Matemática Aplicada (LAC/INPE), São José dos Campos - São Paulo, Brazil, margarete, reinaldo@lac.inpe.br
[3]Divisão de Geofísica Espacial (DGE/INPE), São José dos Campos - São Paulo, Brazil, odim@dge.inpe.br

Abstract: In this work, we propose to test the robustness of Gradient Pattern Analysis (GPA) on such cases performing a threshold reduction of the wavelet coefficients, analyzing how GPA interprets the reconstructed series based on these coefficients. For this, we use a multiresolution analysis decomposition performed by discrete biorthogonal wavelet transforms and a thresholding based on L^2 norm conservation on well known chaotic dynamical systems data sets. GPA is a tool to characterize asymmetry and detect irregular fluctuations in spatio-temporal data. Some efforts have been done to test the GPA strength on the identification of these features.

Keywords: wavelet analysis, gradient pattern analysis, multiresolution analysis, asymmetry measurement.

1. INTRODUCTION

In the last 25 years, wavelet techniques have become an important tool for local data analysis in different areas of science [1, 3, 4, 6, 8, 9]. It's well known that the magnitude of the wavelet coefficients, obtained by the discrete wavelet transform (DWT), depends on the local regularity of the function (or signal) in study[1]. Therefore, to choose the significant wavelet coefficients is a function-dependent problem in the wavelet domain. These significant coefficients could be used in a compact representation of the signal. [2] is an example of the many works that have being done in this sense. One question that arises is if the asymmetries existent in the original signal are preserved in the signal generated by the Inverse Discrete Wavelet Transform (IDWT) applied to this compact wavelet representation, i.e., the reconstruction of the signal using only the significant wavelet coefficients. It's expected that Gradient Pattern Analysis, a technique that measures the fluctuation degree along a signal to quantify its asymmetry and complexity, can be used in this investigation. Some other applications using wavelet analysis combined with GPA are presented in [10]. Since GPA is very sensitive in detecting changes in the signal asymmetric behavior [11], a significant change in GPA measure should indicate a loss of information about the dynamics of the signal.

The following section describes, based on the work of [5], the theoretical background on multiresolution analysis (MRA), highlighting biorthogonal MRA and its main properties that support our proposal. Next, an overview of Gradient Pattern Analysis is given, and the full methodology combining the two techniques is described in Section 4. The results and concluding remarks are presented, respectively, in Sections 5 and 6.

2. MULTIRESOLUTION ANALYSIS

The Multiresolution Analysis $\mathbb{L}^2(\mathbb{R})$ $\{V^j, \phi\}$, called MRA $\{V^j, \phi\}$, is a sequence of linear sub-spaces V^j of $\mathbb{L}^2(\mathbb{R})$ and a associate function ϕ, called scale function. They satisfy the following conditions:

1. $\cdots \subset V^{-1} \subset V^0 \subset V^1 \subset \cdots$, $\quad \cap_{j\in\mathbb{Z}} V^j = \{0\}$, $\mathbb{L}^2(\mathbb{R}) = \overline{\cup_{j\in\mathbb{Z}} V^j}$,
2. $f(x) \in V^j \Leftrightarrow f(2x) \in V^{j+1}$;
3. $f(x) \in V^0 \Leftrightarrow f(x-k) \in V^0, \forall k \in \mathbb{Z}$;
4. $\phi(x-k)_{k\in\mathbb{Z}}$, is a Riesz base of V^0.

Follows, that:

- there is a sequence $h \in \ell^2$ so that the following scale relation holds $\phi(x) = 2\sum_{k\in\mathbb{Z}} h(k)\phi(2x-k)$, where $h(k)$ are called scale coefficients;
- for each j, the family $\phi_k^j(x) = 2^{j/2}\phi(2^j x - k), k \in \mathbb{Z}$, forms a Riesz base of V^j.

In the frequency domain, the scale relation is expressed by $\hat{\phi}(\xi) = H(\xi/2)\hat{\phi}(\xi/2)$, where $H(\xi) = \sum_{k\in\mathbb{Z}} h(k)e^{-ik\xi}$ is the scale filter associate to ϕ. The filter H is a low-pass filter, *i.e.*, $H(0) = 1$ and $H(\pi) = 0$. For more details in MRA see [1].

The main contribution of the theory wavelet is the characterization of the complementary spaces between two embedded spaces $V^j \subset V^{j+1}$, by direct sum $V^{j+1} = V^j + W^j$.

Moreover, the spaces W^j will contain the difference in the information between the resolution levels j and the more refine level $j+1$. There is more than one way to representate this direct sum. In the next section, a method to construct the W^j is presented in the context of an MRA biorthogonal.

2.1. MRA Biorthogonal

A MRA biorthogonal, herein MRAb, is a pair of $\{V^j, \phi\}$ and $\{V^{*\jmath}, \phi^*\}$ of MRA related by $\mathbb{L}^2(\mathbb{R}) = V^0 + V^{*0\perp}$, so that their associated scale functions ϕ e ϕ^* satisfy the following the biorthogonal condition

$$\langle \phi(.-k), \phi^*(.-\ell)\rangle := \int \phi(x-k)\ \phi^*(x-\ell)\ dx = \delta_{k,\ell}, \quad (1)$$

and by so, they are called dual scale functions. Similarly, for a fix $\jmath$, the families $\{\phi_k^\jmath\}$ and $\{\phi_k^{*\jmath}\}$ are also biorthogonal, *i.e.*

$$\langle \phi_k^\jmath, \phi_\ell^{*\jmath}\rangle = 2^\jmath \int \phi(2^\jmath x - k)\ \phi^*(2^\jmath x - \ell)\ dx = \delta_{k,\ell}, \quad (2)$$

In the frequency domains, one has $\sum_k \hat{\phi}(w + 2\pi k)\overline{\hat{\phi}^*(w+2\pi k)} \equiv 1$, where the overbar indicates the complex conjugate. This expression is a direct consequence of the Poisson summation formula.

2.2. Wavelet Functions

Let us consider $W^\jmath = V^{j+1} \cap V^{*j\perp}$ and $W^{*\jmath} = V^{*j+1} \cap V^{j\perp}$. The following direct sum are valid:

$$V^{j+1} = V^j + W^j, \quad V^{*j+1} = V^{*j} + W^{*j}. \quad (3)$$

Defining the functions ψ e ψ^* as

$$\psi(x) = 2\sum_{k\in\mathbb{Z}} g(k)\phi(2x-k), \quad \psi^*(x) = 2\sum_{k\in\mathbb{Z}} g^*(k)\phi^*(2x-k), \quad (4)$$

where usually $g(k) = (-1)^{k+1}h^*(-k+1)$ and $g^*(k) = (-1)^{k+1}h(-k+1)$, one can prove that the families

$$\psi_k^\jmath(x) = 2^{j/2}\psi(2^j x - k), \quad \psi_k^{*\jmath}(x) = 2^{j/2}\psi^*(2^j x - k), \quad (5)$$

are Riesz bases of W^j and W^{*j}. The filters $G(\xi) = \sum_{k\in\mathbb{Z}} g(k)e^{-ik\xi}$ and $G^*(\xi) = \sum_{k\in\mathbb{Z}} g^*(k)e^{-ik\xi}$ are band pass filters, *i.e.*, $G(0) = G^*(0) = 0$ e $G(\pi) = G^*(\pi) = 1$. In frequency domain the scale relations, presented in 4, are expressed by

$$\hat{\psi}(\xi) = G(\xi/2)\hat{\psi}(\xi/2), \quad \hat{\psi}^*(\xi) = G^*(\xi/2)\hat{\psi}^*(\xi/2). \quad (6)$$

The function ψ_k^j are called wavelet functions, and ψ_k^{*j} are called dual wavelet functions. They satisfy the following biorthogonal conditions:

$$\langle \phi_k^\jmath, \psi_\ell^{*\jmath}\rangle = 0, \quad \langle \phi_k^{*\jmath}, \psi_\ell^\jmath\rangle = 0, \quad \langle \psi_k^{*\jmath}, \psi_\ell^m\rangle = \delta_{\jmath,m}\delta_{k,\ell}. \quad (7)$$

The so called families of Daubechies orthogonal wavelet are a particular case of the biorthogonal families when $\phi = \phi^*$ and $\psi = \psi^*$. Another example are the splines biorthogonal wavelets ψ^*, where ψ^* are spline functions.

2.3. Approximation schemes

A MRAb is a usefull tool to study $\mathbb{L}^2(\mathbb{R})$ functions. Functions $f \in \mathbb{L}^2(\mathbb{R})$ can be approximate by projections in V^j such that $\mathcal{P}^j f(x) = \sum_k \langle f, \phi_k^{*\jmath}\rangle \phi_k^\jmath(x)$, or projection in W^j, $Q^j f(x) = \sum_k \langle f, \psi_k^{*\jmath}\rangle \psi_k^\jmath(x)$, since they contain the difference of the information between the levels j and $j+1$, *i.e.*, $Q^j f(x) = [\mathcal{P}^{j+1} - \mathcal{P}^j]f(x)$. Therefore,

$$\mathcal{P}^{j+1} f(x) = [\mathcal{P}^j + Q^j]f(x), \quad (8)$$

corresponds to the decomposition $V^{j+1} = V^j + W^j$. In multilevel $j_0 < j$, we have:

$$\mathcal{P}^{j+1} f(x) = [\mathcal{P}^{j_0} + Q^{j_0} + \cdots + Q^j]f(x), \quad (9)$$

that is associate to the decomposition $V^{j+1} = V^{j_0} + W^{j_0} + \cdots + W^j$. Defining $c_k^j = \langle f, \phi_k^{*\jmath}\rangle$, and $d_k^j = \langle f, \psi_k^{*\jmath}\rangle$, Eq. 8 can be written as

$$\sum_k c_k^{j+1}\phi_k^{j+1}(x) = \sum_k c_k^j \phi_k^j(x) + \sum_k d_k^j \psi_k^j(x), \quad (10)$$

and in multilevel, we have the following formula

$$\sum_k c_k^{j+1}\phi_k^{j+1}(x) = \sum_k c_k^{j_0}\phi_k^{j_0}(x) + \sum_{m=j_0}^{j}\sum_k d_k^m \psi_k^m(x), \quad (11)$$

that corresponds to $\{\phi_k^{j+1}\} \leftrightarrow \{\phi_k^{j_0}\} \cup \{\psi_k^{j_0}\} \cdots \cup \{\psi_k^j\}$. These operations are performed by the discrete wavelet transform $\mathsf{DWT}=\mathsf{DWT}_{j_0}^{j+1}$ and its inverse $\mathsf{IDWT}=\mathsf{IDWT}_{j_0}^{j+1}$, *i.e.*

$$\{c^{j+1}\} \underset{\mathsf{IDWT}}{\overset{\mathsf{DWT}}{\rightleftarrows}} \{c^{j_0}, d^{j_0}, \cdots, d^j\}$$

2.4. Properties

In this section we describe the main properties of the wavelet transform discussed in this work. More details in these properties could be obtained in [1, 18].

2.4.1 Double Localization

In the point of view of these properties of double localization the wavelet coefficients d_k^j are a measure of the frequencial information in $\xi \in \Omega^j$ in the support of $\psi_k^j(t)$. Consequently, the wavelet transform is a time-frequency transform with temporal resolution inversely proportional of the frequencial one, *i.e.*

$$\Delta^j x \times \Delta^j \xi = \text{constant}.$$

The following paragraphs describe briefly how this transform works in the physical and frequencial domain.

Physical Localization: Usually the scale function $\phi(x)$ have a compact support, with length Δx. As j increase, $\phi(2^j x - k)$ is localized in smaller intervals, $\Delta^j x = O(2^{-j})$. The indexes k indicate a translation $k\,2^{-j}$ that are also effectuated. Therefore, in each level j, all the functions have the same shape, changing only the position where they are localized, they change by a integer number multiply by the scale. The wavelet functions have the same behavior.

Frequency Localization: As discussed in this section, the scale families are constructed in terms of the low-pass filter $H(\xi)$. Consequently, a Fourier transform $\hat{\phi}(\xi)$ is symmetrically localized in a region centered in $\xi = 0$.

In this way, in the convolution operation $\hat{\phi}(\xi)$ could be interpreted as a low-pass band filter. If we change the scale, we have $\hat{\phi}(2^{-j}\xi)$ as also a low-pass band filter centered in $\xi = 0$, with bandwidth proportional to 2^j. In the wavelet case we have a different behavior. Usually, $\hat{\psi}(\xi)$ is also a symmetric function, but it is zero in $\xi = 0$. For $\xi > 0$, we have a concentration in a region Ω of length $\Delta\xi$. Therefore, the convolution operations $\hat{\psi}(\xi)$ can be interpreted as pass-band filter, that enhance frequencies $|\xi| \in \Omega$. When we change the scale the changes in $\hat{\psi}(2^{-j}\xi)$ works also as a pass-band filter, with a localization in the region Ω^j, and bandwidth $\Delta^j\xi$, proportional to 2^j.

2.4.2 Approximation order: Polynomial reproduction

In a MRAb the scale function ϕ e it dual ϕ^* must satisfy the Strang–Fix condition (SFC) [17]. Let p be the order of the SFC that ϕ satisfy, *i.e.*, all polynomial of degree p can be represented exactly by $\phi(x)$ and its translates $\phi(x-k)$. It can be verify that p+1 is exactly the multiplicity of the zero in the filter $H(\xi)$ in $\xi = \pi$. This property assure the approximation order

$$||f - \mathcal{P}^j f||_{\mathbb{L}^2} = \mathcal{O}(2^{-j(p+1)}).$$

The same is valid to the dual ϕ^*. If p^* is the order of SFC of ϕ^*, then the multiplicity of the zero in $H^*(\xi)$ em $\xi = \pi$ is $p^* + 1$.

2.4.3 Null moments: polynomial cancellation

On the other hand, as $G(\xi) = e^{-i\xi}\overline{H^*(\xi + \pi)}$, the zero multiplicity of the filter $G(\xi)$, in $\xi = 0$, is equal to $p^* + 1$. Similarly, as $G^*(\xi) = e^{-i\xi}\overline{H(\xi + \pi)}$, is the multiplicity of the zero in the filter $G^*(\xi)$, in $\xi = 0$, is equal to $p + 1$.

We can verify that the number of null moments of one wavelet function is equal to the multiplicity of zeros of the filter $G(\xi)$ in $\xi = 0$. Therefore,

$$\int x^\ell \psi(x)\ dx\ =\ 0, \qquad \ell = 0, \ldots, p^*, \tag{12}$$

that is related by

$$\frac{d^\ell \hat{\psi}(\xi)}{d\xi^\ell}\ |_{\xi=0} = 0, \qquad \ell = 0, \cdots,\ p^*. \tag{13}$$

Similarly, for the dual wavelet ψ^*:

$$\int x^\ell \psi^*(x)\ dx\ =\ 0, \qquad \ell = 0, \ldots, p, \tag{14}$$

that is related by

$$\frac{d^\ell \hat{\psi}^*(\xi)}{d\xi^\ell}\ |_{\xi=0} = 0, \qquad \ell = 0, \cdots,\ p. \tag{15}$$

2.4.4 Local regularity characterization

In the wavelet analyze function can represented in the MRA spaces by expansion in the scale functions or expansion in the wavelet functions.

As is presented in the next theorem the amplitude of the wavelet coefficients $d_k^j = \langle f,\ {\psi_k^*}^j \rangle$ are directly related to the local smoothness of the function f, in the support of ${\psi_k^*}^j$, and the number of null moments of ψ^*. Therefore, wavelet coefficients can be used as local indicators of regularity of the analzed function. Usually these coefficients smaller in the smooth regions. For this reason, expansion in wavelet bases are advantageous for the compression point of view.

Theorem: Let p be the order of SFC of ϕ. If f is a function with continue derivatives $f^{(s)}$ in the support ${\psi^*}_k^j$, $0 \leq s \leq p + 1$, then the wavelet coefficient $d_k^j = \langle f,\ {\psi_k^*}^j \rangle$ and holds the estimation

$$|d_k^j| \leq\ \ C\ \ 2^{-j(s+1/2)}\ \ \| f^{(s)} \|_\infty \tag{16}$$

where C is a constant that depends on ψ^* and the norm $\| f^{(s)} \|_\infty$ in the support of ${\psi^*}_k^j$.

2.4.5 Null moments $\times$ Smoothness

The degree of smoothness of the scale function is directly related to the SFC order, *i.e.*, the smoothness of ϕ, and consequently ψ, grows with p. Therefore, as larger is the smoothness of ψ, as larger is the number of null moments of ψ^*.

Focus in this paradigm null moments/smoothness of the wavelet functions, the interpretation of the following forms the representation can be different:

$$f \ = \ \sum_{j,k} \langle f, {\psi_k^*}^j \rangle \psi_k^j, \tag{17}$$

$$= \ \sum_{j,k} \langle f, \psi_k^j \rangle {\psi_k^*}^j. \tag{18}$$

If ψ^* has more null moments that ψ, then, ψ is much more smooth than ψ^*. Therefore, the first form seams to be much more appropriated to compress the information than the second one, when the reconstruction is made using only the wavelet coefficients d_k^j greater than a certain threshold chosen.

2.5. How to choose the threshold

One question that arises is about what can be considered a small amplitude for the wavelet coefficients. There are several methodologies to decide what is the best threshold (see, for instance, [2]). On the discrete biorthogonal wavelet transform theory, there is not an Energy Conservation Theorem, the so called Parseval's Theorem present in Fourier Analysis, *i.e.*, in MRA Biorthogonal, the summation of all squared signal samples is not necessarily equal to the summation of all scale and wavelet coefficients. So, as an alternative strategy, we use the mean square error (the so called RMSE) to measure the degradation of the signal after gradually removing the smallest detail coefficients.

3. GRADIENT PATTERN ANALYSIS

The Gradient Pattern Analysis (GPA) [12–15] is an innovative technique, which characterizes patterns based on large and small amplitude fluctuations of the spatial, temporal, and spatio-temporal structures represented as a static or dynamical gradient lattice. In this approach, each local fluctuation is represented by a vector in two-dimensional space. Thus, according to [16], a given scalar field of fluctuations can be represented as a composition of four gradient moments: g_1, the integral representation of the fluctuation distribution (vectors); g_2, the integral representation of the corresponding norms; g_3, the integral representation of corresponding phases; and g_4, the complex representation of the gradient pattern (a complex coefficient composed by each corresponding pair of norm and phase). Considering the sets of local norms and phases as discrete compact groups, spatially distributed in a square lattice, the gradient moments have the basic property of being globally invariant (for rotation and modulation).

To calculate the asymmetry coefficient, first of all, the time series must be converted into a mesh grid, rearranging the points in a $n \times n$ array, that we call the 2-D representation of the data. Next, we compute the local fluctuation between each pair of neighboring amplitudes in the global pattern, characterized by its gradient vector. It makes the relative values between adjacent amplitudes to become relevant, rather than the respective absolute values. Such relative values can be characterized by each local vector norm and its orientation (phase). In this approach, each local fluctuation is represented by a vector in a two-dimensional space, composing what we call the gradient lattice. Since symmetric fluctuations are expected to be reflected by symmetric vectors, i.e., vectors with the same norm and opposite phases, the next step consists in eliminating all the symmetric vectors. This operation guarantees that a completely symmetric pattern presents no asymmetric correlation and, thus, no asymmetric vectors. In this case, by definition, g_1 is null. If there are remaining asymmetric vectors, the geometric connection among the fluctuations is generated by a Delaunay triangulation, taking the last point of each vector as a vertex. To measure the asymmetry correlation, called here asymmetry coefficient, we take $g_1 = |\varepsilon - f|/f$, where f is the number of asymmetric fluctuations and ε is the geometric energy correlation given by the number of connections among all fluctuations.

Although this is not the scope of this work, the method can be easily extended to two-dimensional data, by just skipping the first step – generation of the mesh grid – and computing the gradient vectors over the original square matrix.

We present here GPA applied in two examples of short time series composed of only 64 points each. Fig. 1(a) shows a symmetric series generated by a sine function, and Fig. 1(a) shows the same series with some perturbations. We can see in the gradient lattice (Fig. 1,b) that every gradient vector has a symmetric one associated, meaning that all vectors will be removed, giving a null asymmetry coefficient.

In the series presented in Fig. 2(a), we note the presence of some level of asymmetry. Thus, we expect to find a positive value for g_1. In Fig. 2(b) the respective gradient lattice is shown. The few perturbations added in this series are reflected in the gradient lattice, decreasing the number of symmetric vectors to be removed in comparison with the sinusoidal example. Consequently, there are remaining vectors (Fig. 2, c) to generate the triangulation field, shown in Fig. 2(d), which gives $\varepsilon = 98$ and $f = 38$. Taking $g_1 = |\varepsilon - f|/f$, we obtain for this example $g_1 = 1.57$.

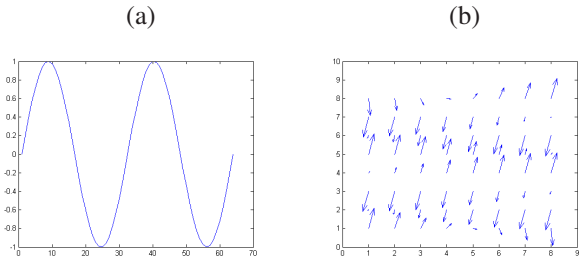

Figure 1 – A symmetric time series composed by 64 points (a) and its respective gradient lattices (b). All gradient vectors are removed, thus the triangulation field does not exist for this case.

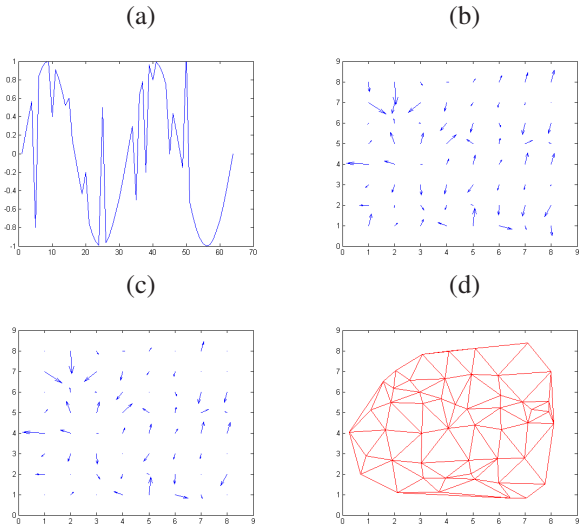

Figure 2 – GPA of two examples of an asymmetric time series composed with 64 points (a). The gradient lattice is shown in (b), and (c) shows the remaining vectors after the symmetric vectors remotion; (d) corresponds to the triangulation field.

Due to the possible changes in the phases of each fluctuation (a vector in the gradient lattice), the parameter ε is very sensitive in detecting local asymmetric fluctuations on the gradient lattice [11]. Several calculations on random patterns have shown that the parameter g_1 quantifies the level of asymmetric fluctuations and it is much more sensitive and precise in characterizing irregular fluctuations than the correlation length measures [11]. When there is no asymmetric correlation in the fluctuation pattern, the total number of asymmetric vectors is zero and then, by definition, g_1 is null. For a random and totally disordered fluctuation pattern, g_1 has the highest value. For a complex pattern composed by

locally asymmetric fluctuations, g_1 is nonzero, defining different classes of irregular fluctuation patterns. Note that for more regular and low frequency fluctuations the triangulation field captures an increase of regularity in the gradient lattice.

4. DATA AND METHODOLOGY

In this study, we performed an exploratory analysis applying DWT with families $\{\psi^*, \psi\}$ with $p^* = 1$ e $p = 3$, *i.e.*, 4 null moments for ψ^* and 2 null moments for ψ, and also the associate representation $\{\psi, \psi^*\}$, in two well known signals provided by the simulation of dynamical processes. These data come from the so called Lorenz Equations (Lz) and Kuramoto-Sivashinsky system (KS). Lz is composed by three ordinary differential equations and used as a simple mesoscale meteorological model. We use one of the variables whose phase space presents a chaotic regime. Fig. 3 shows the signal used in our analysis, sampled with 1024 points and generated by Lz simulation.

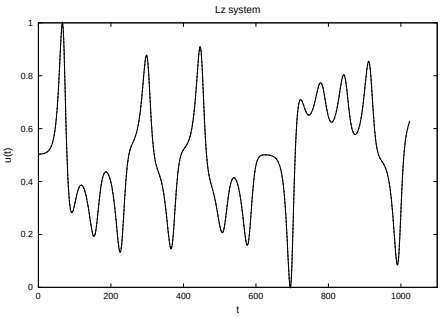

Figure 3 – Signal generated by Lorenz equation.

Used to model processes dynamics, KS has chaotic regime and is represented by a fourth degree partial differential amplitude equation, that can be written as:

$$\frac{\partial u}{\partial t} = -\left[\frac{\partial^2 u}{\partial x^2} + \nu \frac{\partial^4 u}{\partial x^4} + \frac{\partial u^2}{\partial x}\right], \qquad (19)$$

where ν is a viscosity damping parameter and $u = u(x,t)$, with $u(x,t) = u(x + 2\pi, t)$ and periodic boundary conditions. This equation is used as a model for intrinsic instabilities in complex fluids. Details in KS can be found in [7]. The signal used in our analysis, also sampled with 1024 points, is shown in Fig. 4

As discussed above, the DWT is perfectly inverted by the IDWT. Thus, if we apply the transform, eliminate the smallest amplitude wavelet coefficients and perform the IDWT, the result must be close to the original signal. After that, we compare the asymmetry coefficient obtained for the original signal to that measured over the reconstructed one, called here compact wavelet representation. The methodology steps are summarized in Fig. 5.

As shown in the diagram above, we also use the Root Mean Squared Error (RMS) to verify how far the reconstructed series are from the original one.

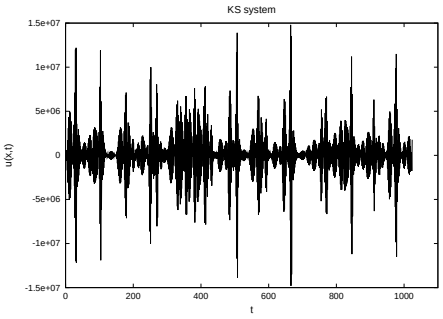

Figure 4 – Signals generated by Kuramoto-Sivashinsky system.

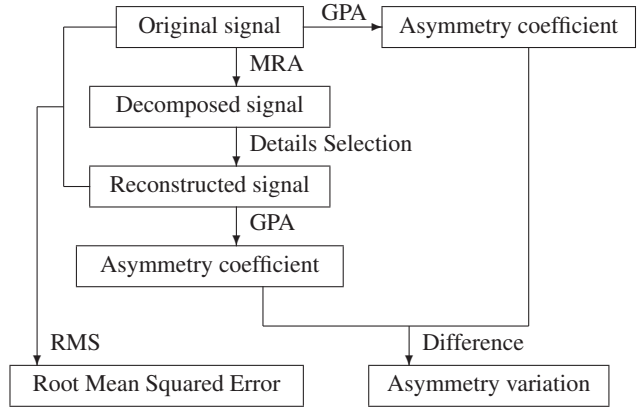

Figure 5 – Diagram illustrating the methodology.

5. RESULTS AND DISCUSSION

Gradually increasing the threshold, defined at each iteration as the minimum absolute amplitude of the signal, we generated a set of asymmetry variations and plotted them for Lz and KS series. Fig. 6 presents the asymmetry variation against the RMSE values measured over the Lz signal reconstructed in each compactness degree. According to [11], asymmetric matrices, where $f \geq 400$, with size about 32×32, can be compared when the standard deviation of the gradient asymmetry coefficient is of the order 10^{-3}.

The compactness degree is supposed to be directly proportional to the signal degradation. Thus, as long as the signal is degraded, as expected, the asymmetry coefficient g_1 gets more distant from the one measured over the original series, what in Lz series seems to go faster beyond analysis functions characterized by a higher number of null moments in the decomposition phase, given here by families {3,1} and {5,1}. The opposite behavior is observed for KS series, as shown in Fig. 7, probably due to the anti-persistent behavior of KS series, which makes its compact wavelet representation more dependent on the high frequency information contained in the detail coefficients. In fact, although Lz and KS represent chaotic systems, they are intrinsically different. While the KS variability is generated from a single state variable, the Lz variability comes from a set of three

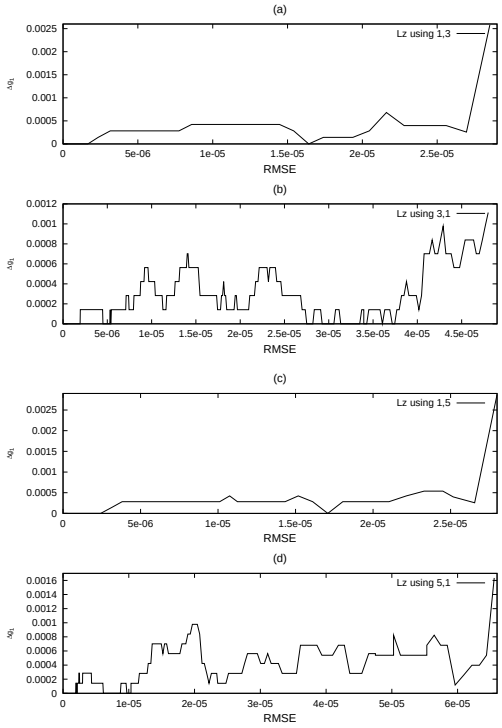

Figure 6 – Asymmetry coefficient variation along increasing root mean squared error for Lz series reconstructed using families {1,3}, {3,1}, {1,5} and {5,1}.

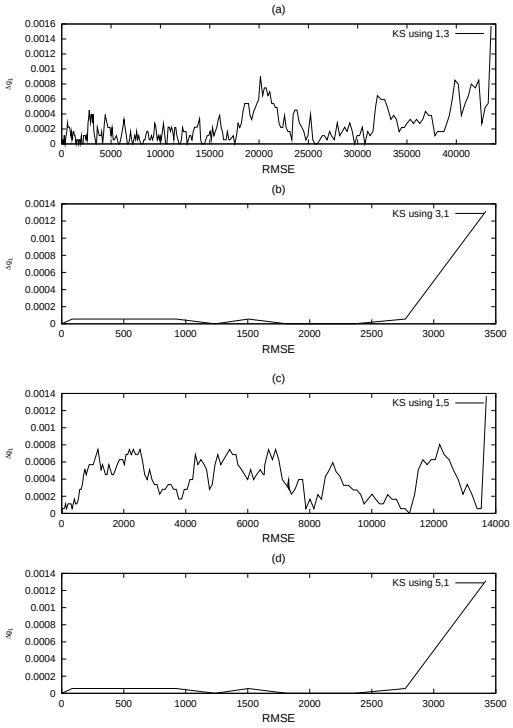

Figure 7 – Asymmetry coefficient variation along increasing root mean squared error for KS series reconstructed using families {1,3}, {3,1}, {1,5} and {5,1}.

state variables.

No apparent significant changes can be observed in both reconstructed (degraded) series, even with high values for RMSE in KS case. Nevertheless, the asymmetry variation is high enough to loose its accuracy. Fig. 8 shows the difference $|KS - KS_{rec}^{\{5,1\}}|$, where KS is the denomination for the original series, and $KS_{rec}^{\{5,1\}}$ relates to KS series reconstructed using {5,1} analysis function.

Note that, as shown in Fig. 9, for the Lz system, there are much more "disregarded" structures than to KS.

It's also relevant to consider the rate of significant points necessary to produce a compact wavelet representation with no loss of information in the context of the asymmetries and irregular fluctuations measured by GPA. Table 1 shows the minimum number of significant points for each function analysis.

Table 1 – Number of significant points.

Series	**{1,3}**	**{3,1}**	**{1,5}**	**{5,1}**
Lz	95.14%	47.81%	95.12%	23.60%
KS	70.06%	48.97%	83.90%	49.17%

The most remarkable result is about reconstruction of Lz signal using family {5,1}. As we can see in the table above, this analysis function is able to reconstruct Lz series using only 23.51% of the detail coefficients, with no loss of information of the characteristic nonlinear underlying process. As said before, it can be associated to the persistent behavior of Lz dynamics, comparing to the anti-persistent variability of KS process.

6. FINAL REMARKS

Our promising results indicate that, with some improvements, the method can be used to indicate the robustness of GPA and work as an additional tool for measuring asymmetry more efficiently. One of the improvements and additional analysis that can be done in our methodology, already evolving to be published soon, includes to incorporate other families of the same orders analyzed here, say {2,4}, {3,3}, with order 6, and the fourth order {2,2}.

Finally, by comparing the results for KS and Lz, it is clear that higher order decomposition has enhanced the coefficients reduction in KS series, while higher order reconstruction has enhanced coefficients reduction in Lz series. In practice, this behavior indicates that, for different chaotic dynamics, one can find different biorthogonal families more appropriated to represent each one with maximum compactness. In order to verify such dependence, a complementary analysis which does include other chaotic dynamics will be performed, and research along these lines is currently in progress.

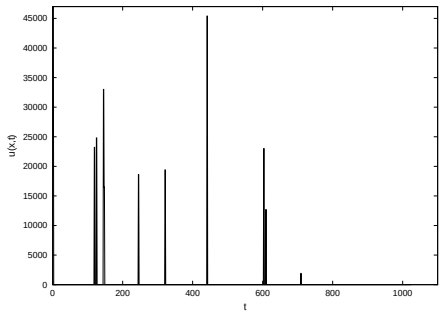

Figure 8 – Absolute difference between the original KS series amplitude values and the ones obtained by its reconstruction using family {5,1}.

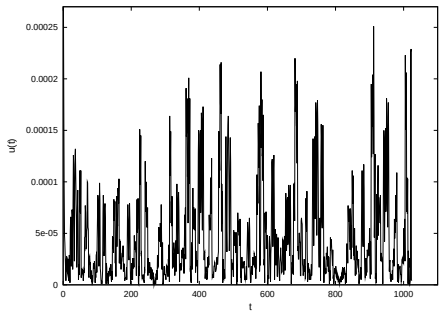

Figure 9 – Absolute difference between the original Lz series amplitude values and the ones obtained by its reconstruction using family {5,1}..

ACKNOWLEDGMENTS

The authors would like to thank CNPq and FAPESP for the financial support. Authors also thank Murilo S. Dantas and Erico Rempel for the simulation datasets.

REFERENCES

[1] I.Daubechies. *Ten Lectures on Wavelets*, SIAM, 1992.

[2] A.Azzalini, M.Farge and K.Schneider, *Nonlinear wavelet thresholding: A recursive method to determine the optimal denoising threshold*, Appl. Comput. Harm. Anal., 18, 177-185, 2005.

[3] M.Farge, *Wavelet transforms and their applications to turbulence*, Annu. Rev. Fluid Mech. 24, 395-457, 1992.

[4] F.I.M.Argoud, F.M.de Azevedo, J.Marino Neto, *Comparative study concerning to wavelet functions and its different applicabilities to pattern recognition in electroencephalogram*, Revista Brasileira de Engenharia Biomédica 20 (2-3), 49-59, 2004.

[5] M.O.Domingues, *Análise Wavelet na simulação numérica de equações diferenciais parciais com adaptabilidade espacial*, IMECC, Unicamp, Brazil, october 2001 (Portuguese).

[6] M.O.Domingues, O.Mendes, A.M.da Costa, *On wavelet techniques in atmospheric sciences*, Advances in Space Research 35 (5), 831-842, 2005.

[7] A.C.-L.Chian, E.L.Rempel, E.E.Macau, R.R.Rosa, F.Christiansen, *High-dimensional interior crisis in the Kuramoto-Sivashinsky equation*, PRE 65, 035203(4), 2002.

[8] K.Hosoda, H.Kawamura, *Examination of the merged sea surface temperature using wavelet analysis*, Journal of Oceonography 60, 843-852, 2004.

[9] J.E.Fowler, D.N.Fox, *Embedded wavelet-based coding of three-dimensional oceanographic images with land masses*, IEEE Transactions on Geoscience and Remote Sensing 39 (2), 2001.

[10] R.R.Rosa, M. Karlický, T.B. Veronese, N.L. Vijaykumar, H.S. Sawant, A.I. Borgazzi, M.S. Dantas, E.B.M. Barbosa, R.A. Sych, O. Mendes. *Gradient pattern analysis of short solar radio bursts*, Advances in Space Research, 42, 844-851, 2008.

[11] R. R. Rosa, A. S. Sharma, J. A. Valdivia, *Characterization of asymmetric fragmentation patterns in spatially extended systems*, Int. J. Mod. Phys. C 10, 147-163, 1999.

[12] R. R. Rosa, A. S. Sharma, J. A. Valdivia, H. S. Sawant, *Characterization of localized turbulence in plasma extended systems*, Physica A 257, 509-514, 1998.

[13] F. M. Ramos, R. R. Rosa, C. R. Neto, A. Zanandrea, *Generalized complex entropic form for gradient pattern analysis of spatio-temporal dynamics*, Physica A 283, 171-174, 2000.

[14] A. T. Assireu, R. R. Rosa, N. L. Vijaykumar, J. A. Lorenzetti, E. L. Rempel, F. M. Ramos, L. D. Abreu Sá, M. J. A. Bolzan, M.J.A., A. Zanandrea, *Gradient pattern analysis of short nonstationary time series: an application*, Physica D 168 (1), 397-403, 2002.

[15] M. P. M. A. Baroni, R. R. Rosa, A. F. Silva, I. Pepe, L. S. Roman, F. M. Ramos, R. Ahuja, C. Persson, E. Veje, *Modeling and gradient pattern analysis of irregular SFM structures of porous silicon*, Microelectr. J. 37 290-294, 2006.

[16] R. R. Rosa, M. R. Campos, F. M. Ramos, S. Fujiwara, T. Sato, *Gradient pattern analysis of structural dynamics: application to molecular system relaxation*, Braz. J. Phys. 33, 605-609, 2003.

[17] Strang, G.; G. A. Fix, A Fourier analysis of finite element method, Bulletim American Mathematics Society,28(2):288-305,1993.

[18] Domingues, M. O., Gomes, S.M., Cortina, E., Biorthogonal wavelets applied to METEOSAT image compressing, *Wavelet and Aplications II*, Szu,

H. H., Apr #" 17–21,",SPIE, Orlando, FL,2491:726–733,1995.

[19] S.Wolfram, *A new kind of science*, Wolfram Media, 2002.

[20] P.D. Dresselhaus, Y. Chong, J.H. Plantenberg, and S.P. Benz, *Stacked SNS Josephson Junction Arrays for Quantum Voltage Standards*, IEEE Transactions on Applied Superconductivity Vol. 13, No. 2, pp. 930-933, June 2003.

[21] Y. Chong, C. J. Burroughs, P. D. Dresselhaus, N. Hadacek, H. Yamamori, and S. P. Benz, "Practical High-Resolution Programmable Josephson Voltage Standards using Double- and Triple-Stacked $MoSi_2$-Barrier Junctions," to appear in IEEE Trans. Appl. Supercond., Vol. 15, No. 2, June 2005.

[22] G. M. Rocha, G. A. Kyriazis, "A Software for the Evaluation of the Stability of Measuring Standards Using Bayesian Statistics", Proceedings of the 13^{th} International Symposium on Measurements for Industry Applications, pp 386-391, Athens, September 2004.